

CRITICAL HEAT FLUX ANALYSIS OF DIVERTOR COOLING FLOW CHANNEL IN FUSION REACTOR WITH CFD METHOD

by

Xiangyu LI^a, Guanghui WANG^b, Yun GUO^{a*}, and Songwei LI^c

^a School of Nuclear Science, University of Science and Technology of China, Hefei, China

^b China Ship Development and Design Center, Wuhan, China

^c State Key Laboratory of Reactor System Design Technology, Nuclear Power Institute of China, Chengdu, China

Original scientific paper

<https://doi.org/10.2298/TSCI210216203L>

Situated at the bottom of the vacuum vessel, the divertor extracts heat and ash produced by the fusion reaction, minimizes plasma contamination, and protects the surrounding walls from thermal and neutronic loads. The vertical targets of divertor are designed to be able for up to 20 MW/m² high heat flux. It is a great ordeal for both the material performance and the cooling ability. Critical heat flux margin is very crucial during the design of divertor. The ANSYS FLUENT is used in this paper to predict the critical heat flux on a monoblock structure with a twisted tape inside the tube. Numerical results are validated with the corresponding sets of experimental results. In this paper, CFD method used to predict critical heat flux of divertor cooling channel was first introduced. On the other hand, influence of inlet subcooling on critical heat flux is studied in detail. The inlet subcooling affect the critical heat flux much complicated for the single-side heated and swirl flow channel. Whether the influencing trend or the locations of critical heat flux occurrence are different under different inlet subcooling. The derivations between the simulation and experimental results were no more than 32%. This study proves the CFD tools can provide efficient help on the understanding of the critical heat flux phenomenon of complex construction.

Key words: critical heat flux, diverter, swirl flow, inlet subcooling, CFD

Introduction

Plasma facing components (PFC) is designed to be subjected to unexpected high heat fluxes (HHF) in the harsh tokamak environment. As it shows in fig. 1. The thermal load on different parts of divertor is varied. The heat flux sustained by the international thermonuclear experimental reactor (ITER) divertor vertical targets is estimated at 10 MW/m² (steady-state) and 20 MW/m² (slow transients). Divertor vertical target is illustrated in fig. 2. The divertor vertical targets have (2 inner + 2 outer) put together 8-11 plasma-facing units which are hydraulically connected in parallel. The carbon fiber cloth (CFC) monoblock of outer vertical target (OVT) is shown in fig. 2, in which twisted tape is used to increase margins against critical heat flux (CHF). Once unexpected high heat flux occurred, it will cause materials failure which may lead to serious damage. Thus, heat removal ability of divertor is crucial for a safe operation in future fusion reactor. The CHF, which refers to the burning-out-leading heat flux, is an important parameter to evaluate the cooling ability of a certain cooling system.

* Corresponding author, e-mail: guoyun79@ustc.edu.cn

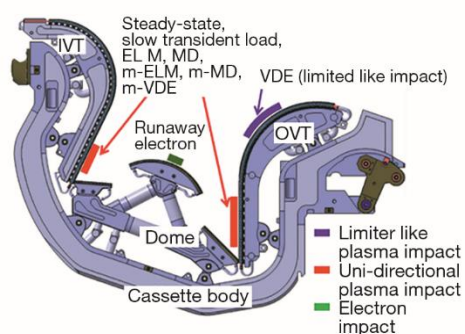


Figure 1. Thermal event impact; m - migrated

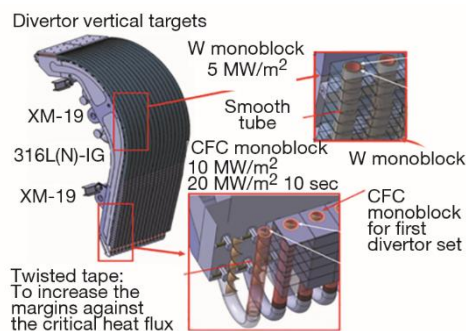


Figure 2. The W monoblock and CFC monoblock

There are many earlier works on boiling heat transfer and CHF [1, 2]. Boscary *et al.* [3] conducted experiments to investigate CHF of water subcooled flow in one-side heated swirl tubes. Experimental results corresponding to various thermal hydraulic conditions are reasonably well predicted by a correlation deduced from a sublayer dry out model. Yagov *et al.* [4] studied heat transfer and crisis in swirl flow boiling. Based on experimental measurements, they found that CHF at one-side heating in swirl flow is essentially higher than that under uniform heating condition. Dedov *et al.* [5] conducted experiments in swirl flow under one-side heating conditions. Appropriate calculation formulas are derived. France *et al.* [6] developed a thermodynamic non-equilibrium model for a two-phase, vapor and liquid-drop, dispersed swirl flow in a vertical tube with a twisted-tape insert. The post-CHF swirl flow heat transfer is analyzed and compared with experimental data. Liu *et al.* [7] developed a theoretical CHF prediction model for the subcooled flow boiling based on the liquid sublayer dry out mechanism. The model also shows good adaptation to non-uniform heating, twist tape insert and non-water (nitrogen and refrigerant 113) system. Hegde *et al.* [8] studied experimentally pool boiling heat transfer characteristics of Al_2O_3 -water nanofluids using a NiCr test wire of 36 standard wire gauge diameter, CHF with different volume concentrations of nanofluid is obtained. Previous study uses traditional experimental method and empirical correlation to study the CHF phenomenon, however, CFD approach which is the most promising method is applied in this study recently.

During plasma operation, divertor is confronting energetic plasma particles, neutron irradiation and some slow transient thermal load. Thus, the target plates of divertor are under extreme thermal loads. Around the world, a great effort has been devoted to optimization of channel geometry and CHF prediction through expensive experiments. The ITER organization has launched a HHF test aimed to study the performances of materials and components under harsh conditions [9]. Ezato *et al.* [10] completed a series of experiments to detect the CHF of a screw tube under different flow conditions and with different materials. Together with four ITER home teams, Raffray *et al.* [11] have studied the CHF performance of different CHF enhancement with geometries including porous coating, screw tubes and swirl tape configuration. Di Maio *et al.* [12] performed a comparative evaluation study on three different options for the cooling circuit layout of the divertor PFC with a qualified CFD code. At the same time, Courtois *et al.* [13] used a creative acoustic method to detect the CHF on a CFC monoblock tube with swirl tape. Considering nearly all the experiments are costly and do not give much detailed information, numerical method is an efficient way to provide assistance.

This work aims to obtain the CHF and boiling heat transfer characteristics of divertor cooling flow channel in fusion reactor with CFD method and provide reference for structural optimum design of divertor. Hence, this paper uses CFD method to model the CHF in a CFC monoblock tube based on the Courtois's research and a simple comparison is performed. Additionally, the detailed heat flux partition, flow and temperature fields are analyzed. Furthermore, influences of inlet velocity and subcooling on CHF are also studied.

Physical and numerical models

Physical models [14]

Eulerian multiphase model is able to distinguish different phases and solve their governing equations separately. As well as interfacial models that describe the interfacial momentum and energy interaction and extended wall boiling models that describe the heat transfer between wall and fluid, it can simulate the multiphase flow and heat transfer well.

Turbulence models

Renormalization group (RNG) k - ε turbulent model is used to model the turbulence. The k represents the turbulent kinetic energy and ε represents the turbulent dissipation rate. The governing equations for the k - ε model are:

$$\frac{\partial}{\partial t}(\rho k) + \frac{\partial}{\partial x_i}(\rho k u_i) = \frac{\partial}{\partial x_j} \left[\left(\mu + \frac{\mu_t}{\sigma_k} \right) \frac{\partial k}{\partial x_j} \right] + G_k + G_b - \rho \varepsilon - Y_M + S_k \quad (1)$$

$$\frac{\partial \varepsilon}{\partial t}(\rho \varepsilon) + \frac{\partial}{\partial x_i}(\rho \varepsilon u_i) = \frac{\partial}{\partial x_j} \left[\left(\mu + \frac{\mu_t}{\sigma_\varepsilon} \right) \frac{\partial \varepsilon}{\partial x_j} \right] + C_{1\varepsilon} \frac{\varepsilon}{k} (G_k + C_{3\varepsilon} G_b) - C_{2\varepsilon} \rho \frac{\varepsilon^2}{k} + S_\varepsilon \quad (2)$$

where G_k represents the generation of turbulent kinetic energy due to the mean velocity gradients, G_b – the generation of turbulent kinetic energy due to buoyancy, and Y_M – the contribution of the fluctuating dilatation in compressible turbulence to the overall dissipation rate. The $C_{1\varepsilon}$, $C_{2\varepsilon}$, and $C_{3\varepsilon}$ are model constants, σ_k and σ_ε are the turbulent Prandtl numbers for k and ε , respectively, and S_k and S_ε are the source term.

Governing equations

Introducing subscript q for the q^{th} phase, the generalized phase governing equations following the same forms.

– Conservation equation

$$\frac{\partial}{\partial t}(\alpha_q \rho_q) + \nabla(\alpha_q \rho_q \bar{v}_q) = \sum_{q=1}^n (\dot{m}_{pq} - \dot{m}_{qp}) + S_q \quad (3)$$

– Momentum equation

$$\begin{aligned} \frac{\partial}{\partial t}(\alpha_q \rho_q \bar{v}_q) + \nabla(\alpha_q \rho_q \bar{v}_q \bar{v}_q) = & -\alpha_q \nabla p + \nabla \bar{\tau}_q + \alpha_q \rho_q \bar{g} + \\ & + \sum_{q=1}^n (\bar{R}_{pq} + \dot{m}_{pq} \bar{v}_{pq} - \dot{m}_{pq} \bar{v}_{pq}) + (\bar{F}_q + \bar{F}_{\text{lift},q} + \bar{F}_{\text{vm},q}) \end{aligned} \quad (4)$$

– Energy equation

$$\frac{\partial}{\partial t}(\alpha_q \rho_q h_q) + \nabla(\alpha_q \rho_q \bar{v}_q h_q) = -\alpha_q \frac{\partial p}{\partial t} + \bar{\tau}_q \nabla \bar{v}_q - \nabla \bar{q}_q + S_q + \sum_{p=1}^n (Q_{pq} + \dot{m}_{pq} h_{pq} - \dot{m}_{qp} h_{qp}) \quad (5)$$

Extended wall boiling models

The heat flux from wall to fluid, q_w , is divided into two parts: q_l refers to the part transferred to liquid and q_v refers to that transferred to vapor. Moreover, q_l is also divided into three parts: liquid phase convective heat flux, q_c , quenching heat flux, q_q , and evaporation heat, q_e .

$$q_w = f(\alpha_l)(q_c + q_e + q_q) + [1 - f(\alpha_l)]q_v \quad (6)$$

where $f(\alpha_l)$ means the area ratio of liquid area that the heating wall transfers heat to, which is defined:

$$f(\alpha_v) = 1 - f(\alpha_l) = \begin{cases} 0 & \alpha_v < \alpha_{v,1} \\ \frac{1}{2} \left[1 - \cos \left(\pi \frac{\alpha_v - \alpha_{v,1}}{\alpha_{v,2} - \alpha_{v,1}} \right) \right] & \alpha_{v,1} \leq \alpha_v \leq \alpha_{v,2} \\ 1 & \alpha_v > \alpha_{v,2} \end{cases} \quad (7)$$

The extended Rensselaer Polytechnic Institute model gives the following expressions of the four heat flux components.

– Liquid phase convective heat flux

$$q_c = h_l(T_w - T_l)A_l \quad (8)$$

– Quenching heat flux

$$q_q = \frac{2\sqrt{k_l \rho_l C_{p,l}}}{\sqrt{\pi T}}(T_w - T_l) \quad (9)$$

– Evaporation heat flux

$$q_e = V_d N_w \rho_v h_{lv} f \quad (10)$$

– Vapor phase convective heat flux

$$q_v = h_v(T_w - T_v)(1 - A_l) \quad (11)$$

There are also some other auxiliary models listed as follows.

Area occupied by liquid is defined:

$$A_l = \min \left(1, \eta \frac{\pi}{4} N_w D_w^2 \right) \quad (12)$$

Where the empirical coefficient, η , is defined [15]:

$$\eta = 4.8 \exp\left(-\frac{Ja_{\text{sub}}}{80}\right) \quad (13)$$

Jacob number is:

$$Ja_{\text{sub}} = \frac{\rho_l C_{p,l} \Delta T_{\text{sub}}}{\rho_v h_{lv}} \quad (14)$$

Bubble departure frequency [16]:

$$f = \sqrt{\frac{4g(\rho_l - \rho_v)}{3\rho_l D_w}} \quad (15)$$

Bubble nucleate density based on wall's subcooling is defined [17]:

$$N_w = 210^{1.805} (T_w - T_{\text{sat}})^{1.805} \quad (16)$$

Bubble departure diameter based on an empirical correlation [18]:

$$D_w = \min[0.0014, 0.0006e^{(T_{\text{sat}} - T_w)/45.0}] \quad (17)$$

Interfacial models

Interfacial mass transfer model

The mass transfer procedure during boiling includes two parts: liquid near the heat wall evaporation and the bubble condensation in the subcooled mainstream.

– Mass transfer from the wall to vapor:

$$\dot{m}_e = \frac{\dot{q}_e}{h_{lv} + C_{p,l} \Delta T_{\text{sub}}} \quad (18)$$

– Interfacial mass transfer:

$$\dot{m} = \dot{m}_{lt} + \dot{m}_{vt} = \frac{\dot{q}_{lt} + \dot{q}_{vt}}{h_{lv}} \quad (19)$$

Interfacial momentum transfer models

In boiling flow, the most important momentum transfer forces may include drag, lift, and turbulent drift forces, some other forces are also can be included. Their definitions list as follows:

– Drag force [19]

$$\vec{F}_D = \frac{C_D \mu_l A_{if} \text{Re}}{8d_v} (\vec{v}_v - \vec{v}_l) \quad (20)$$

Where the C_D is the coefficient of drag force and A_{if} is the interfacial area defined:

$$A_{if} = \frac{6\alpha_v(1 - \alpha_v)}{d_v} \quad (21)$$

- Lift force [20]

$$\vec{F}_L = -C_L \rho_l (1 - \alpha_v) (\vec{v}_l - \vec{v}_v) (\nabla \vec{v}_l) \quad (22)$$

- Turbulent dispersion force [21, 22]

$$\vec{F}_{td,i} = -\vec{F}_{td,j} = C_{TD} \frac{C_D \mu_l \mu_{t,l} A_{if} \text{Re}}{8 d_v \rho_l \sigma_{lv}} \left(\frac{\nabla \alpha_v}{\alpha_v} - \frac{\nabla \alpha_l}{\alpha_l} \right) \quad (23)$$

- Wall lubrication force [23]

$$\vec{F}_{wl} = C_{wl} \rho_l \alpha_l \left| \vec{v}_{l,z} - \vec{v}_{v,z} \right|^2 \vec{n}_w \quad (24)$$

- Virtual mass force [20]

$$\vec{F}_{vm} = C_{vm} \alpha_p \rho_q \left(\frac{d_q \vec{v}_q}{dt} - \frac{d_p \vec{v}_p}{dt} \right) \quad (25)$$

Interfacial energy transfer models

- Interface to liquid heat transfer

As bubbles departure from the heat wall and move to the subcooled regions, the heat transfer to the liquid is:

$$\dot{q}_{lt} = h_{lt} (T_{sat} - T_l) \quad (26)$$

where h_{lt} is based on the Ranz-Marshall correlation [24, 25]:

$$h_{lt} = \frac{k_l}{d_v} (2 + 0.6 \text{Re}^{0.5} \text{Pr}^{0.33}) \quad (27)$$

- Interface to vapor heat transfer

According to Lavieville *et al.* [26] the vapor is assumed to retain the saturation temperature and the formulation is:

$$\dot{q}_{vt} = \frac{\alpha_v \rho_v C_{p,v}}{\delta t} (T_{sat} - T_v) \quad (28)$$

where δt is the time scale and is default set to be 0.05 seconds in ANSYS FLUENT.

Modelling and numerical method

The details of the experimental apparatus and measurements are given by Courtois *et al.* [13]. The experiment was intended to detect the CHF and simulate the thermal behavior of an OVT of ITER divertor. The channel tube with twisted tape (turbulence promoter) have exactly the same geometry as a real OVT monoblock. The geometry of numerical analysis was identical with only the experimental test section which is showed in fig. 3. The heat blocks are made up of 11 connected 20.0 mm × 20.0 mm × 20.0 mm blocks and only the central 5 blocks were exposed to a uniform single-side heat flux. The outer diameter (OD) of the tube is 14.0 mm and inner diameter (ID) is 12.0 mm. The spacing of twisted tape is 28 mm as shown in fig. 3(b). There is a 0.8 mm thick swirl tape exists in part of the flow channel and it

fits closely to the inner tube wall. Both the heat blocks, tube wall and swirl tape are made of CuCrZr.

For better convergence, less calculation cost and high mesh quality, structure mesh generation method was taken. In order to make sure the simulation independent on mesh size, grid sensitivity analysis was conducted under a one-phase condition with flow rate 2.7 m³ per hour. Pressure drops and flow direction velocity were compared, as shown in tab. 1 and fig. 4. As the node number increases, results differ littler. When Mesh 2 is changed to Mesh 3, pressure drop differs much less than 0.1 % and velocity profile nearly coincides. Hence, Mesh 2 is considered optimal for this simulation. Figure 5 shows the mesh of solid domain and fig. 6 refers to the mesh of inner fluid and swirl tape. The average grid size of Mesh 2 is about 0.5 mm for the whole section and for the near wall region is about 0.2 mm. Total mesh grid number is about 2.220.000.

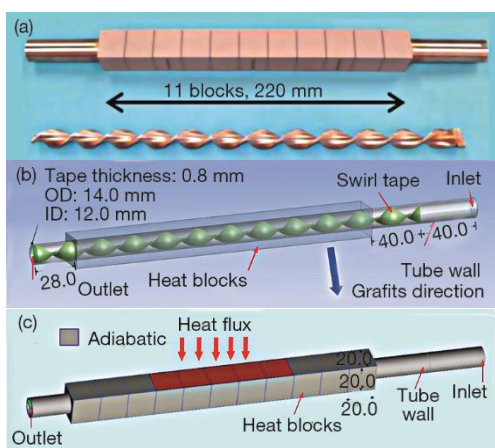


Figure 3. Schematic diagram of the test section; (a) experimental physical map [13], (b) perspectives for swirl tape, and (c) thermal boundary schematic

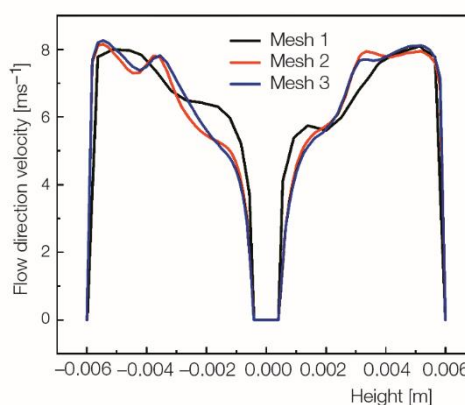


Figure 4. Flow direction velocity profiles along center line of outlet

Table 1. Grid sensitivity analysis

Mesh	Nodes	Cells	Pressure drop [Pa]
Mesh 1	1295474	1456690	75897.2
Mesh 2	1806612	2010693	76325.5
Mesh 3	2398092	2631251	76341.3

Within ANSYS FLUENT, the Eulerian multiphase model, some other interfacial models and the mixture RNG *k-ε* turbulent model are considered. To solve the governing equations as well as the auxiliary equations, the pressure-velocity coupling is solved with coupled method and the gradient is discretized by least squares cell-based method. All the other variables are discretized by first order upwind method. All these calculations are performed on the Windows 7 Professional 64-bit OS and the CPU is Intel Xeon E5-2697 at 2.7GHz with 48 processors and 64 GB of memory. On this condition, it may take one week to finish a single calculation case.

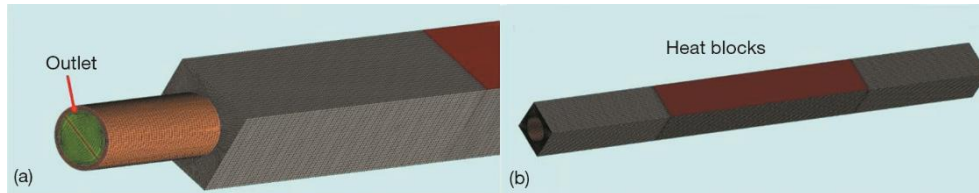


Figure 5. Outside and heat blocks mesh

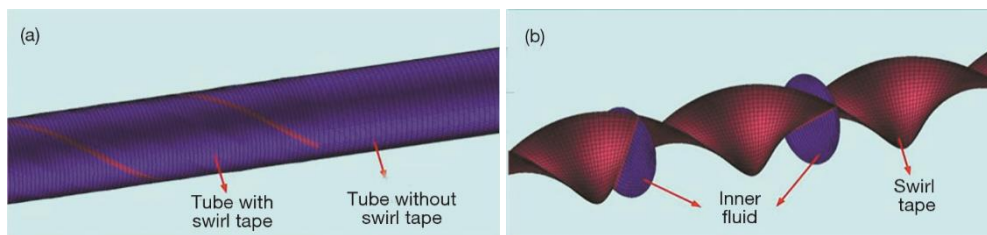


Figure 6. Inner fluid and swirl tape mesh

Results and discussions

Experimental results [13]

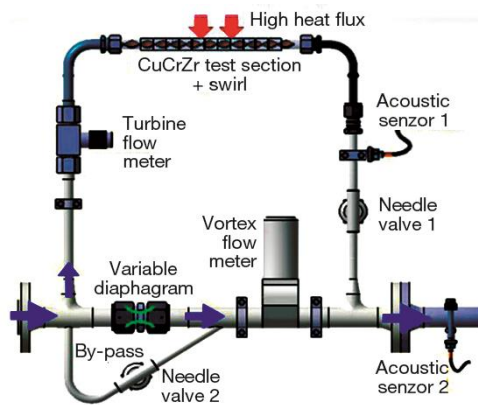


Figure 7. Experimental test facility

The experiment was carried out under 3.0 MPa under which the saturation temperature is 507 K, the coolant inlet temperature is 363.15 K (the subcooling degree is 144 K) and the testing apparatus is shown in fig. 7. An electron beam (EB) gun is used as heating source, which simulates the plasma thermal load to test the power handling capabilities of the test section. A parallel channel is used to adjust the ratio of test section flow rate to the total flow rate, it is called dilution rate and defined as $(Q_T + Q_B)/Q_T$ in the original paper, where Q_T [m^3h^{-1}] is test section flow rate and Q_B [m^3h^{-1}] is by-pass flow rate. According to the acoustic test method, CHF under different test cases have been detected. All concerning information is summarized in tab. 2.

Table 2. Experimental information summarization [13]

Test number	#1	#2	#3	#4
Test section flow rate, [m^3h^{-1}]	2.8	2.7	1.4	0.7
By-pass flow rate, [m^3h^{-1}]	2.8	10.8	12.6	12.6
Dilution rate	2	5	10	19
CHF detection, [MWm^{-2}]	28.4	35.0	24.0	17.6

Based on the experimental results, it can be found the dilution rate would affect the CHF a lot even under a similar mass-flow rate. The CHF value decreases with a decreasing inlet mass flow rate.

The CFD simulation results

To detect CHF through numerical simulation, there were usually several methods. Zhang *et al.* [27] predicted CHF based on the rapid increase of local wall temperature with ANSYS FLUENT. Ashouri *et al.* [28] numerically investigated turbulent force convective heat transfer of water-based Al₂O₃ nanofluid flowing through the CuCrZr cooling tube of a small scale of mock up made of five tungsten monoblocks using single phase model.

Koncar *et al.* [29] have done much work to validate NEPTUNE_CFD through several DNB experiments. Within the NEPTUNE_CFD Code, the heat flux partition factor $f(\alpha_i)$ was defined by Lavieville [26] model . In which the critical void fraction is 0.8 and the local void fraction equal to 0.8 was used as the criterion for CHF occurrence in Koncar’s study. However, in ANSYS FLUENT the factor $f(\alpha_i)$ is modelled by Tentner [30], the critical value $\alpha_{v,1}$ is 0.9 and $\alpha_{v,2}$ is 0.95 in the definition expression. In earlier study [31], it can be found that whether the local void fraction reached 0.9 or local temperature rapid increase was regarded as the criteria of CHF occurrence; it did not make much difference. In this paper, the former criteria was selected. Similar to the experiment, uniform heat flux was added on the heating surface marked red as fig. 3(c) and other faces was adiabatic. During calculation, the uniform heat flux was increased step by step. While approaching the criteria of CHF, a relatively small step was increased. The velocity inlet condition keeps 6.63 m/s and the pressure outlet condition keeps 3.0 MPa. The simulation results compared with experiment were listed in the tab. 3.

Table 3. The CFD simulation results and experiment results comparison

Case	Flow rate [m ³ h ⁻¹]	Dilution rate	CHF experiment [MWm ⁻²]	CHF simulation [MWm ⁻²]	Derivation	Pressure drop [kPa]
#2	2.7	5	35.0	33.0	5.7%	79
#3	1.4	10	24.0	19.0	20.8%	22
#4	0.7	19	17.6	12.0	31.8%	6.4

For the previous results, the CFD simulation gave a little bit lower CHF value and the derivation became larger while the experimental flow rate decreases and dilution rate increases. However, it can be seen that in the experiment, tab. 2, there was a multiple channel paralleled with the test section and a larger dilution rate did affect the CHF value to a higher value under the acoustic method. The simulation considered the test section only and the difference between the simulation and the experimental results should be relatively lower. The pressure drops among the three cases nearly follow the $\Delta P \sim v^2$ rules. The maximum deviation is 31.8%. Considering the error of the traditional CHF experimental correlation is generally more than 30% [3, 4, 32], the accuracy of CFD results is acceptable.

The case for simulating experiment test case #2 is selected to display the simulation details. With the CFD simulation tools, the detailed temperature and velocity fields of the entire test section could be studied. Figure 8 shows the outside temperature of the heating blocks. In this structure, the cooling tube is located in the center of the heating blocks and thus the heat in the block corners couldn’t transfer well, which results that the highest temperature

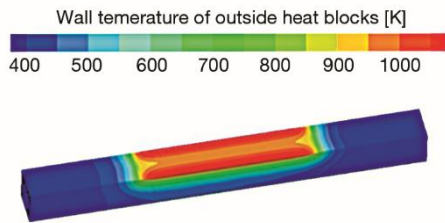


Figure 8. Wall temperature of outside heat blocks

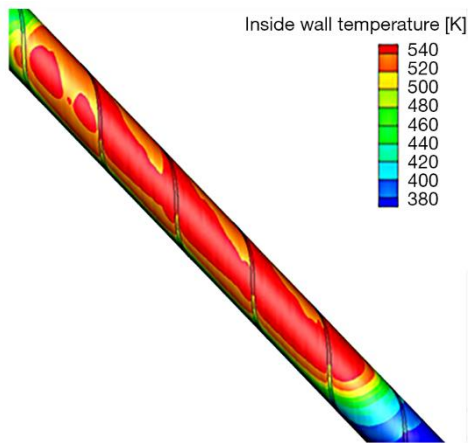


Figure 9. Inside wall temperature

located at the side of the heating face. Figure 9 refers to the wall temperature and fig. 10 shows the fluid temperature at the near wall position. The heat flux partition on different wall is showed as fig. 11. For the existence of solid swirl tape, the local heat conduction at the tube wall was better than the surrounding coolant's heat convection. Thus, the local wall temperature was relatively lower as shown in fig. 9. However, the coolant could carry more heat via convection and have a better cooling ability. So the coolant undertook more heat flux than swirl tape as fig. 12 shows. Both temperature distributions didn't seem like symmetrical as fig. 8 shows. It is mainly because the spiral velocity field as fig. 12 shows. The swirl tape drove the coolant much more turbulent and the heating made this phenomenon more obvious. On this condition, the swirl tape could enhance the cooling ability much. Figure 13 shows the pressure distribution along the tube and the near wall vapor void fraction is showed in fig. 14. The vapor concentrated on the downstream of every swirling flow section, besides, the void fraction on the right side near the twisted tape is larger, because the velocity was relatively lower here and the coolant was heated by twisted tape at the same time. Then, the vapor disappeared due to the subcooled main flow.

The effect of inlet subcoolings

If the valves or pump of the cooling system have something wrong, the inlet fluid temperature may change. Hence, the effect of different inlet subcoolings on CHF has been also studied. The results were summarized in tab. 4. All simulation cases were under same mass flow rate as the experimental test case #2.

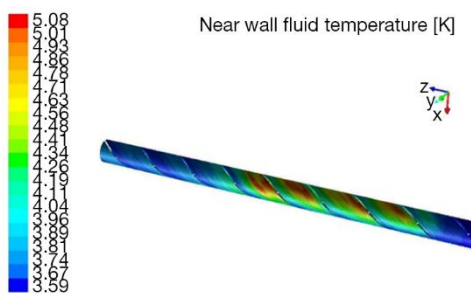


Figure 10. Near wall fluid temperature

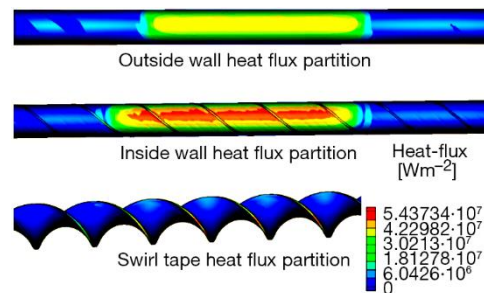


Figure 11. Heat flux partition around tube wall

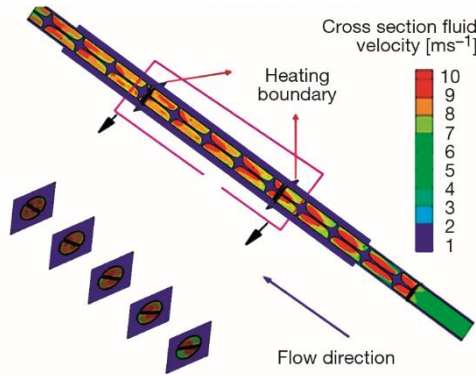


Figure 12. Cross section fluid velocity

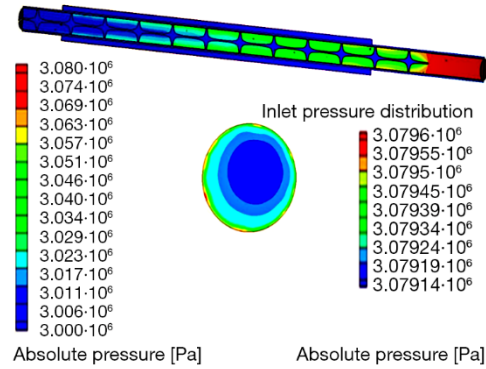


Figure 13. Pressure distribution inside the flow channel

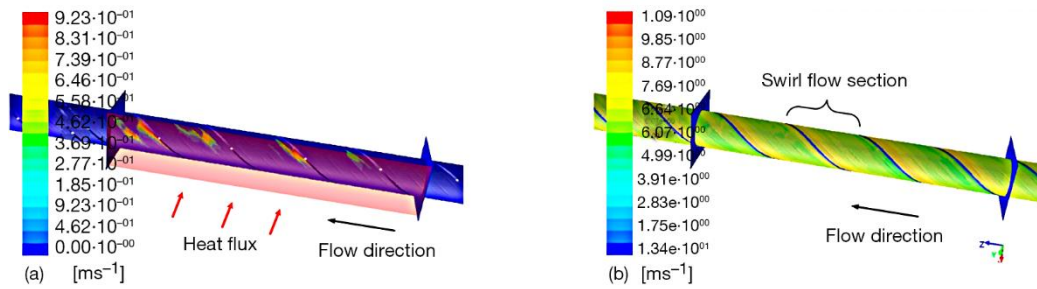


Figure 14. Near wall vapor void fraction (a) and velocity field (b)

Table 4. Inlet subcooling influence for CHF

Case	Subcooling [K]	CHF simulation [MWm^{-2}]	Pressure drop [kPa]
1	144	33.0	79
2	108	24.0	74.6
3	72	20.0	71
4	48	21.4	66
5	36	28.0	68

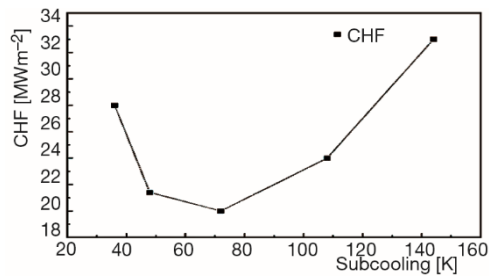


Figure 15. The CHF value varied with subcooling degrees

Based on this simulation results, it can be found the inlet subcooling does not affect CHF linearly. Within the simulation subcooling range (36~144 K), CHF was increased with increasing subcooling for high subcooling and decreased during relatively lower subcooling range (36~72 K), fig. 15.

In a typical vertical flow tube CHF was usually positively correlated with subcooling. However, test section in this research, coolant flow in spiral channel but heated only in a single side. The vapor generated upstream during the heated side would be condensed in the

spiral downstream, which could not be accumulated on the next heating surface. That was the main difference between this spiral test section and typical round flow channel and it possibly changed the effect of subcooling on CHF.

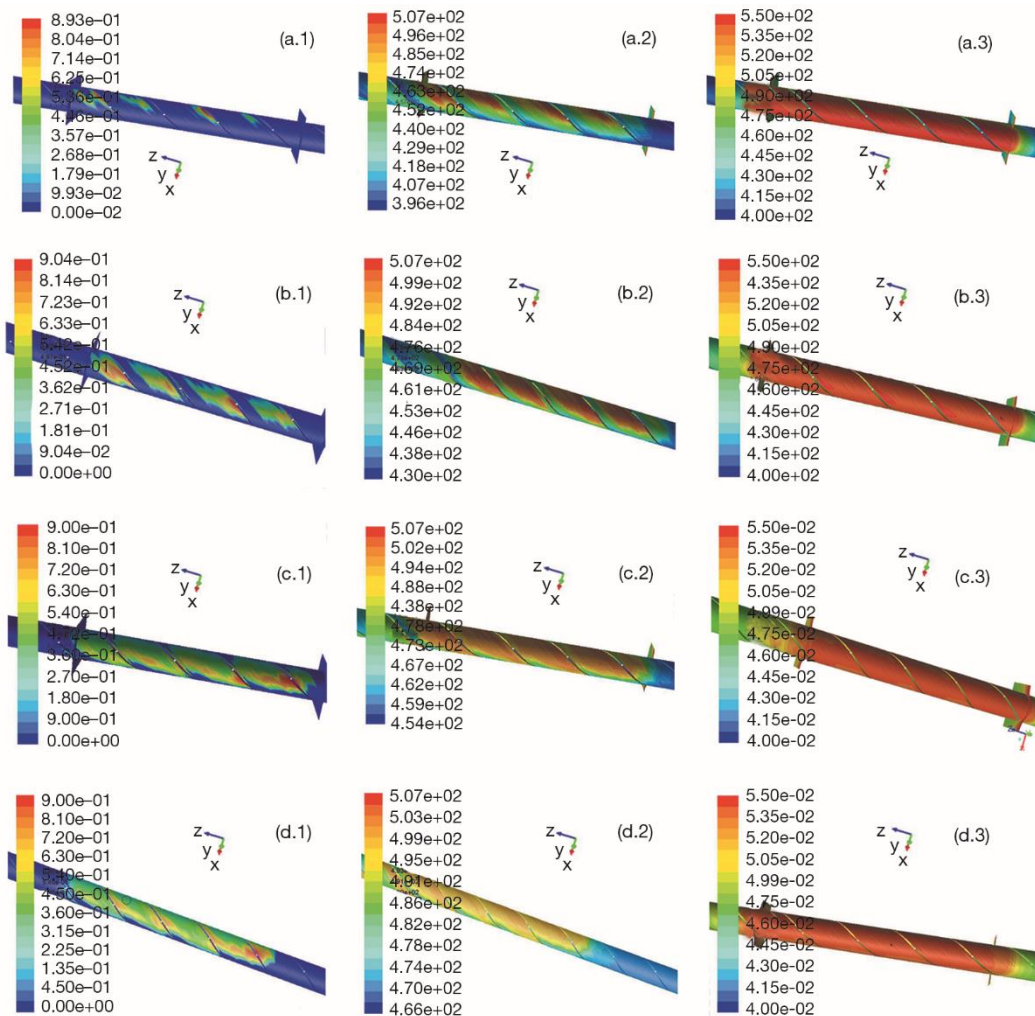


Figure 16. Near wall void fraction fluid and wall temperature on different subcooling. The former letters refer to different inlet subcoolings: a is 108 K, b – 75 K, c – 48 K, and d – 36 K; the latter numbers refer to different quantities: 1 is near wall void fraction, 2 – near wall fluid temperature and 3 – wall temperature. The details of subcooling 144 K are displayed above. In each column, the colorful legend refers to the same numerical range

In this study, it was found that the subcooling did not affect CHF in a single way. A lower subcooling means easier for saturation and vapor generation which helps to the emergence of lower CHF. But at the same time, it also means a wider area would fall into subcooled boiling which is showed in fig. 16. and it could enhance heat transfer and many bubbles will be generator in whole heating surface. It will take the bubbles to the main flow and

prevent the bubbles accumulating partly. Hence, it will increase the CHF value. The detailed explanation is given below.

Figure 16 gives the contrast of near wall void fraction, fluid temperature and wall temperature with different subcooling (108 K, 72 K, 48 K, and 36 K). Comparing the second column in fig. 16 it can be found that, for a lower subcooling case, the near wall fluid temperature spread more uniformly and the maximum temperature is relatively lower. The wall temperature distributes uniformly for both subcooling cases and the higher subcooling case performed a relatively higher wall temperature. Though, the differences among these cases are not much. With the first column figures, it can be easily found for the lower subcooling case, the vapor distributes more widely, which means more subcooled boiling area and helps to enhance the local heat transfer capability. It can explain that the lower subcooling case gives the lower fluid temperature (shown as second column in fig. 16) and wall temperature (shown as third column in fig. 16) even in a higher heat flux. Simultaneously, the near wall void fraction peaks moved to the inlet of heated section for lower subcooling (below 48 K) cases, which means the CHF occurred at the inlet heating section for the case.

The main reason is that for the lower subcooling case, there generating more vapor and the downstream vapor was entrained to the central main flow by the swirling flow field. As showed in fig. 17(a), take the 36 K subcooling case for example, the generated vapor was attached to the surface at the heating inlet position (marked 1), the downstream vapor (marked 2) started to enter to the center and the surface void fraction was relatively lower. In this structure, for an even lower subcooling case, the vapor was easily concentrated in the center as fig. 17(b) shows the 18 K subcooling case and it is hard to detected CHF on the tube wall.

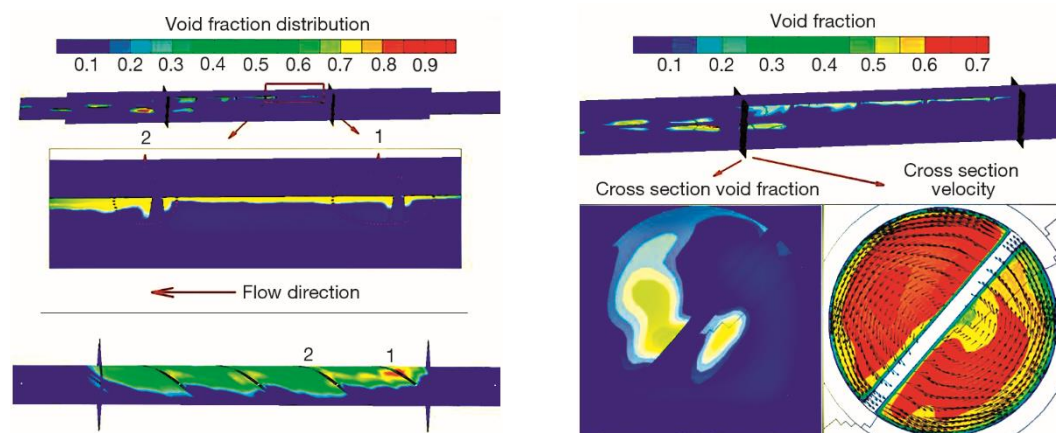


Figure 17. Void fraction distribution inside the tube; (a) 36 K and (b) 18 K

Conclusion

This work validated the ability of ANSYS FLUENT Code in predicting the CHF on a high pressure condition even for such complex geometry system. The derivations between the simulation and experimental results were no more than 32 %. Detailed flow and temperature fields were obtained. The peak temperature in the block located at the heating corner and the vapor concentrated on the right-side downstream of every swirling flow section, besides, the swirl tape could stir the flow field much and enhance the cooling ability. The simulation

with different inlet subcooling proved the effect of subcooling on cooling ability is not on a single level, a lower inlet subcooling cooled system might have a better cooling ability. This work provides reference for structural optimum design of divertors, and more reasonable inlet subcooling could be considered for the future CHF experiments in divertors.

References

- [1] Kamel, M., Lezsovits, F., Boiling Heat Transfer of Nanofluids: A Review of Recent Studies, *Thermal Science*, 23 (2019), 1, pp. 109-124
- [2] Stojanovic, A., et al., Nucleate Pool Boiling Heat Transfer: Review of Models and Bubble Dynamics Parameters, *Thermal Science*, 26 (2021), 1A, pp. 157-174
- [3] Boscary, J., et al., Critical Heat Flux of Water Subcooled Flow in One-Side Heated Swirl Tubes, *International Journal of Heat and Mass Transfer*, 42 (1999), 2, pp. 287-301
- [4] Yagov, V. V., et al., Heat Transfer and Crisis in Swirl Flow Boiling, *Experimental Thermal and Fluid Science*, 29 (2005), 7, pp. 871-883
- [5] Dedov, A. V., et al., Hydrodynamics and Heat Transfer in Swirl Flow Under Conditions of One-Side Heating, Part 2: Boiling Heat Transfer, Critical Heat Fluxes, *International Journal of Heat and Mass Transfer*, 53 (2010), 21-22, pp. 4966-4975
- [6] France, D. M., et al., Analysis of Post-CHF Swirl Flow Heat Transfer, *International Journal of Heat and Mass Transfer*, 37 (1994), Suppl. 1, pp. S31-S40
- [7] Liu, W., et al., Prediction of Critical Heat Flux for Subcooled Flow Boiling, *International Journal of Heat and Mass Transfer*, 43 (2000), 18, pp. 3371-3390
- [8] Hegde, R. N., et al., Flow Visualization and Study of Critical Heat Flux Enhancement in Pool Boiling with Al₂O₃-Water Nanofluids, *Thermal Science*, 16 (2012), 2, pp. 445-453
- [9] Hirai, T., et al., ITER Relevant High Heat Flux Testing on Plasma Facing Surfaces, *Materials Transactions*, 46 (2005), 3, pp. 412-424
- [10] Ezato, K., et al., Critical Heat Flux Experiments Using a Screw Tube Under DEMO Divertor-Relevant Cooling Conditions, *Fusion Engineering and Design*, 83 (2008), 7-9, pp. 1097-1101
- [11] Raffray, A. R., et al., Critical Heat Flux Analysis and Ramped for the Design of the ITER Divertor, *Fusion Engineering and Design*, 45 (1999), 4, pp. 377-407
- [12] Di Maio, P. A., et al., Thermal-Hydraulic Behaviour of the DEMO Divertor Plasma Facing Components Cooling Circuit, *Fusion Engineering and Design*, 124 (2017), Nov., pp.415-419
- [13] Courtois, X. et al., Critical Heat Flux Acoustic Detection: Methods and Application to ITER Divertor Vertical Target Monitoring, *Fusion Engineering and Design*, 88 (2013), 9-10, pp. 1722-1726
- [14] ***, ANSYS FLUENT Theory Guide, ANSYS Inc, Canonsburg, USA
- [15] Del Valle, V. H., Kenning, D. B. R., Subcooled Flow Boiling at High Heat Flux, *International Journal of Heat and Mass Transfer*, 28 (1985), 10, pp. 1907-1920
- [16] Cole, R., A Photographic Study of Pool Boiling in the Region of the Critical Heat Flux, *AIChE Journal*, 6 (1960), 4, pp. 533-542
- [17] Lemmert, M., Chawla, J. M., Influence of Flow Velocity on Surface Boiling Heat Transfer Coefficient, in: *Heat Transfer in Boiling*, (E. Hahne and U. Grigull, Eds.), Academic Press and Hemisphere, New York, USA, 1977
- [18] Tolubinski, V. I., Kostanchuk, D. M., Vapor Bubbles Growth Rate and Heat Transfer Intensity at Subcooled Water Boiling, *Proceedings*, 4th Int. Heat Transfer Conference, Paris, France, 1970
- [19] Ishii, M., Two-Fluid Model for Two-Phase Flow, *Multiphase Science and Technology*, 5 (1990), 1-4, pp. 1-63
- [20] Drew, D. A., Lahey, R. T., *In Particulate Two-Phase Flow*, Butterworth-Heinemann, Boston, Mass., USA, 1993
- [21] Simonin, O., Viollet, P. L., Modelling of Turbulent Two-Phase Jets Loaded with Discrete Particles, *Phenomena in Multiphase Flows*, 1990 (1990), pp. 259-269
- [22] Cole, R., A Photographic Study of Pool Boiling in the Region of the Critical Heat Flux, *AIChE Journal*, 6 (1960), 4, pp 533-542
- [23] Antal, S. P., et al., Analysis of Phase Distribution in Fully Developed Laminar Bubbly Two-Phase Flow, *International journal of multiphase flow*, 17 (1991), 5, pp. 635-652
- [24] Ranz, W. E., Marshall, W. R., Evaporation from Drops, Part I and Part II, *Chemical Engineering Progress*, 4 (1952), pp. 173-180

- [25] Ranz, W. E., Marshall, W. R., Evaporation from Drops, Part I, *Chemical Engineering Progress*, 3 (1952), pp. 141-146
- [26] Lavieville, et al., NEPTUNE CFD V1.0 Theory Manual, EDF, 2005
- [27] Zhang, R., et al., Prediction of CHF in Vertical Heated Tubes Based on CFD Methodology, *Progress in Nuclear Energy*, 78 (2015), Jan., pp. 196-200
- [28] Ashouri, H., et al., Numerical Simulation of Heat Transfer Improvement in the Divertor of Fusion reactors by Using Al₂O₃ Nanofluid, *J. of Theoretical and Applied Physics*, 12 (2018), Dec., pp. 299-308
- [29] Koncar, B., et al., Computational Fluid Dynamics Modeling of Boiling Bubbly Flow for Departure from Nucleate Boiling Investigations, *Multiphase Science and Techn.*, 23 (2011), 2-4, pp. 165-222
- [30] Tentner, A., et al., Advances in Computational Fluid Dynamics Modeling of Two-Phase Flow in a Boiling Water Reactor Fuel Assembly, *Proceedings*, International Conference on Nuclear Engineering, Miami, Fla., USA, 2006
- [31] Wang, G., et al., CFD study on Critical Heat Flux in curved surface, *Proceedings*, NUTHOS-11, HICO, Korea, Paper N11P0095
- [32] Katto, Y., Critical heat flux, *International Journal of Multiphase Flow*, 20 (1994), Suppl. 1, pp. S53-S90